First absolute seasonal temperature estimates for greenhouse climate from clumped isotopes in bivalve shells

Niels de Winter (n.j.dewinter@uu.nl)
Universiteit Utrecht https://orcid.org/0000-0002-1453-5407
Inigo Müller
Universiteit Utrecht
Ilja Kocken
Universiteit Utrecht https://orcid.org/0000-0003-2196-8718
Nicolas Thibault
Universiteit Utrecht
Clemens Ullmann
Universiteit Utrecht
Alex Farnsworth
University of Bristol
Daniel Lunt
University of Bristol
Philippe Claeys
Vrije Universiteit Brussel
Martin Ziegler
Universiteit Utrecht

Article

Keywords: temperatures, controversial, greenhouse, climates

Posted Date: January 4th, 2021

DOI: https://doi.org/10.21203/rs.3.rs-128320/v1

Version of Record: A version of this preprint was published at Communications Earth & Environment on June 10th, 2021. See the published version at https://doi.org/10.1038/s43247-021-00193-9.

First absolute seasonal temperature estimates for greenhouse climate from clumped isotopes in bivalve shells

Niels J. de Winter[1,2]*, Inigo A. Müller[1], Ilja J. Kocken[1], Nicolas Thibault[3], Clemens V. Ullmann[4], Alex Farnsworth[5], Daniel J. Lunt[5], Philippe Claeys[2], Martin Ziegler[1]

[1]Department of Earth Sciences, Faculty of Geosciences, Utrecht University, the Netherlands

[2]AMGC research group, Vrije Universiteit Brussel, Brussels, Belgium

[3]Faculty of Science, IGN, University of Copenhagen, Denmark

[4]Camborne School of Mines and Environment and Sustainability Institute, University of Exeter, UK

[5]School of Geographical Sciences, University of Bristol, UK.

**Corresponding author*

ABSTRACT

Seasonal variability in sea surface temperatures plays a fundamental role in climate dynamics and species distribution. As such, it is essential to better understand seasonal variability in climates of the past. Previous reconstructions of seasonality in deep time are poorly constrained, relying on controversial assumptions such as estimates of seawater composition and neglect seasonal bias. This work presents the first absolute seasonal temperature reconstructions based on clumped isotope measurements in bivalve shells which, critically, do not rely on these assumptions. Our new approach reconstructs highly precise higher mid-latitude (~50°N) monthly temperatures from individual oyster and rudist shells of the Campanian (78 million years ago) greenhouse period (15—27 °C seasonal range). Our analysis demonstrates that seasonal bias and previous assumptions about sea water oxygen isotope composition can lead to highly inaccurate temperature reconstructions, distorting our understanding of the behavior of greenhouse climates and our

ability to model them. Our results agree with fully coupled climate model simulations showing greenhouse climates outside the tropics were warmer and more seasonal than previously thought.

MAIN

Introduction

Seasonal extremes were of vital importance for the evolution and distribution of life over geological history[1]. The effects of greenhouse warming on seasonal variability in temperature and the hydrological cycle are still poorly constrained, while being of considerable interest for projecting future climate and its impact on the ongoing biodiversity crisis[2,3]. Reconstructions of deep time (pre-Quaternary) greenhouse periods yield valuable insights into the dynamics of warm climates and the ecological response to forcing mechanisms such as rising atmospheric CO_2 levels[4,5]. Accurate reconstructions are imperative to evaluate climate model predictions under dissimilar climate states[6], in particular seasonal range for which there is little quantitative evidence to constrain climate model behavior. The warm, ice free Late Cretaceous period presents a valuable reference to assess seasonal variability under greenhouse conditions[7,8].

Reconstructions based on stable oxygen isotope ratios ($\delta^{18}O_c$) in marine carbonates and organic paleothermometry (e.g. TEX_{86}) indicate that Late Cretaceous global mean sea surface temperatures (SST) were ~5-6°C warmer than today with a reduced latitudinal temperature gradient (an "equable climate"[9]), while exhibiting limited temperature seasonality[7,10,11,12]. However, the reliability of past seasonal reconstructions is undermined by poorly constrained assumptions. This hampers our understanding of past warm climates and hinders accurate evaluation of climate models[13,14]. Two potentially significant biases resulting from assumptions

underlying SST reconstructions are seasonal bias and bias resulting from assumed seawater composition ($\delta^{18}O_{sw}$ bias).

Seasonal bias occurs if a proxy is interpreted as representing annual mean conditions but is in fact biased to a particular season. Since fossil species producing the material that constitutes SST archives may not have a close modern relative for proxy calibration[16], uncertainties about their growth seasons may unpredictably bias reconstructions. This bias limits our understanding of the behavior of greenhouse climates, which further leads to misinterpretation of model-data comparisons of past warm climates[15] and hinders the use of paleoclimate data for informing future climate predictions. Seawater oxygen isotope composition ($\delta^{18}O_{sw}$) forms an important input parameter into the widely used carbonate $\delta^{18}O_c$ temperature proxy[17], but remains poorly constrained across geological timescales[18,19]. Biases in assumed $\delta^{18}O_{sw}$ composition thus undermine SST reconstructions.

The advent of carbonate clumped isotope (Δ_{47}) SST reconstructions on a seasonal scale promises to eliminate these two biases[20]. The clumped isotope thermometer yields accurate SST reconstructions independent of $\delta^{18}O_{sw}$ assumptions[21,22]. This technique also allows the reconstruction of $\delta^{18}O_{sw}$, yielding information about the (local) hydrological cycle, an important aspect of climate rarely constrained in deep time, and rectifying bias in the popular carbonate $\delta^{18}O_c$ temperature proxy. Recent advances in clumped isotope instrumentation and standardization have reconciled previous inter-lab disagreements and shown that many carbonate paleoarchives (e.g. foraminifera, bivalves and eggshells) conform to the theoretical Δ_{47} temperature calibration[23,24] (see **Supplementary Methods and Discussion**). The large sample sizes required for individual Δ_{47}-based temperature estimates (>2 mg) have complicated paleoseasonality reconstructions using

this accurate method[25], but a recently developed statistical approach enables its use for seasonality reconstructions[20].

Here we use clumped isotope analyses on microsampled (~100 µg) profiles through fossil bivalve shells to obtain, for the first time, absolute SST and $\delta^{18}O_{sw}$ seasonality reconstructions of a greenhouse climate. We apply this new method on well-preserved oyster (*Rastellum diluvianum* and *Acutostrea incurva*) and rudist (*Biradiolites suecicus*) shells from Campanian (78.1±0.3 Ma[26]) coastal localities of the Kristianstad Basin in southern Sweden (46±3°N paleolatitude[27]; see **Fig. 1** and **METHODS**). We further supplement these reconstructions with fully coupled climate model simulations of the Campanian greenhouse (see **METHODS**) to explore their implications for the "equable climate" hypothesis.

Results

All specimens showed clear seasonal $\delta^{18}O_c$ fluctuations of −2.0–0.0‰ in *R. diluvianum*, -2.0–0.0‰ in *A. incurva* and -2.7‰–-1.0‰ in *B. suecicus* on which shell chronologies were based (see **Methods**). The assumption that periodic $\delta^{18}O_c$ fluctuations reflect seasonality is demonstrated to be a valid basis for constructing intra-shell chronologies in nearly all modern environments[20]. Seasonal $\delta^{18}O_c$ patterns show that the specimens record 3 (*A. incurva* and *B. suecicus*) to 6 (*R. diluvianum*) full years of growth. Clumped isotope analyses on small aliquots yielded Δ_{47} ranges between 0.62–0.73‰ for *R. diluvianum*, 0.64–0.76‰ for *A. incurva* and 0.63–0.75‰ for *B. suecicus*. Summaries of measurement results are displayed in **Table 1**.

Detailed step-by-step results of the data processing routine are shown in **Supplementary Methods** and[20]. **Fig. 2** and **Table 1** show monthly Δ_{47}, SST and $\delta^{18}O_{sw}$ reconstructions for each specimen. Uncertainties at the 95% confidence level on monthly SST vary between 1.8 and 4.2°C

93 owing to variable monthly sampling density related to intra-shell growth rate variability (**Fig. 2**).
94 While growth rate varied through the year (**Fig. 2A**), all monthly time bins in each specimen
95 contained enough datapoints to allow separate monthly SST and $\delta^{18}O_{sw}$ reconstructions.
96 Calculations of mean annual temperature (MAT) and seasonality from these monthly averages
97 eliminates seasonal bias due to growth rate variability. Statistically significant ($p<0.01$) SST
98 seasonality was observed in all specimens. Summer and winter temperatures, defined as mean
99 temperatures of the warmest and coldest month, in *A. incurva* (13±2–26±4°C) and *B. suecicus*
100 (14±4–25±3°C) are statistically indistinguishable ($p>0.2$), while SST from *R. diluvianum* are
101 significantly higher (20±2–29±2°C; $p<0.05$). Significant $\delta^{18}O_{sw}$ seasonality was found in *R.*
102 *diluvianum* (0.0±0.3–1.1±0.3‰VSMOW; $p<0.01$) and *B. suecicus* (-1.8±0.8–0.6±0.5‰VSMOW;
103 $p<0.01$), but not in *A. incurva* (-0.9±0.2–-0.4±0.9‰VSMOW; $p=0.07$; **Fig. 2**; **Table 1**). *R.*
104 *diluvianum* records significantly higher $\delta^{18}O_{sw}$ values ($p<0.01$) than the other specimens. In all
105 specimens, monthly $\delta^{18}O_{sw}$ positively correlates with monthly SST (see **Fig. 2**).
106 We compare our reconstructed SST with local and global Campanian SSTs modelled using
107 the HadCM3L model, one of the most developed paleoclimate models to date and part of the IPCC
108 intercomparison assessment reports[6,14]. We present global Campanian latitudinal gradients in
109 summer, winter and MAT (**Fig. 3A**) as well as monthly SST in the Boreal Chalk Sea (**Fig. 3B**) for
110 both 2× and 4× preindustrial atmospheric pCO_2 simulations (see **Methods**). Model results are
111 summarized in **Supplementary Data 5**. The modelled Campanian latitudinal SST gradient
112 (difference between tropics and high-latitude MAT; 26°C in both simulations) resembles the
113 modern (25°C gradient). Modelled global mean Campanian SST seasonality (difference between
114 warmest and coldest month) is lower (6.6°C) than that of the modern ocean (8.6°C) under 2×
115 preindustrial pCO_2 conditions and similar to the present (8.2°C) in the 4× preindustrial pCO_2

simulation, in disagreement with the hypothesis of reduced seasonality during greenhouse conditions. Campanian modelled MAT is ~18°C and ~22°C under 2× and 4× preindustrial atmospheric pCO_2, respectively, compared to ~14°C in the modern ocean (NOAA, 2020), yielding an equilibrium climate sensitivity, or global warming per doubling of atmospheric CO_2 concentration, of ~4°C[15]. Specifically, simulated seasonal SST ranges in the Campanian Kristianstad Basin of 7±3–20±2°C and 12±2–26±2°C for 2× and 4× preindustrial atmospheric pCO_2 forcing, respectively, are significantly warmer than in present day southern Sweden (3±0.8–17±0.4°C[28]).

Discussion

Our novel Δ_{47}-based monthly SST and $\delta^{18}O_{sw}$ reconstructions from *A. incurva* and *B. suecicus* are statistically indistinguishable from 4× preindustrial pCO_2 simulations ($p>0.05$) and significantly warmer than the 2× preindustrial pCO_2 simulations (>4°C higher MAT, $p<0.05$) of local SST seasonality ($p>0.05$; **Fig. 3**). Higher ($p<0.05$) SST (+4–5°C) and $\delta^{18}O_{sw}$ (+1.0–1.5‰) in *R. diluvianum* are likely caused by local differences in its shallower, inter-tidal (< 5 m) environment[27]. Temporary areal exposure during low tides could have elevated temperatures and $\delta^{18}O_{sw}$ recorded in *R. diluvianum* year-round by direct sunlight and evaporation, as in modern inter-tidal oyster species[29]. By comparison, the deeper (5-15m) subtidal environments of *A. incurva* and *B. suecicus* were unaffected by these processes and may have received more water with an open marine $\delta^{18}O_{sw}$ signature (closer to the -1‰VSMOW assumed for the ice-free Cretaceous[30]), especially in winter. These local environmental differences are not resolved in the climate model simulations but show the unprecedented detail of local SST and $\delta^{18}O_{sw}$ reconstructions from clumped isotope analyses on bivalve shells (see **Supplementary**

Discussion). The ~1‰ $\delta^{18}O_{sw}$ seasonality shows that summers in the Campanian Kristianstad Basin either experienced excess evaporation, which increases $\delta^{18}O_{sw}$ by preferentially removing isotopically light seawater, or reduced precipitation, which supplies isotopically light meteoric water, reducing $\delta^{18}O_{sw}$. Both processes lead to comparatively dry summers and wet winters.

Strong seasonal fluctuations in $\delta^{18}O_{sw}$ (up to 1.3‰ in *B. suecicus*) and regular deviations from the commonly assumed -1‰VSMOW $\delta^{18}O_{sw}$ value[26] lead to large differences (up to 8.9°C in *R. diluvianum*) between SST estimates based on Δ_{47} and the widely used $\delta^{18}O_c$ proxy (**Fig. 2**). The risk of assuming constant $\delta^{18}O_{sw}$ is even more clearly illustrated by significantly (+3.5–6.0°C) higher $\delta^{18}O_c$-based seasonal temperature reconstructions for *B. suecicus* compared to *A. incurva*, while both specimens grew under similar SST seasonality conditions (**Fig. 2B**). Similarly, $\delta^{18}O_c$-based temperature reconstructions of *A. incurva* and *R. diluvianum* are indistinguishable, while the paleoenvironment of *R. diluvianum* was 4–5°C warmer year-round (**Fig. 2B**), illustrating that the constant $\delta^{18}O_{sw}$ assumption is only valid in settings with negligible $\delta^{18}O_{sw}$ seasonality and where $\delta^{18}O_{sw}$ is known. Low-latitude Tethyan SST seasonality reconstructions based on rudist $\delta^{18}O_c$[10] agree with model simulations, which may indicate that $\delta^{18}O_{sw}$ seasonality is less important in open marine settings, although data–model agreement is by no means solid evidence for correct $\delta^{18}O_{sw}$ assumptions, which should always be independently verified (**Fig. 3A**). Our findings corroborate previous Δ_{47}-based and proxy comparison studies which also report a significant cold bias (~-8°C) in $\delta^{18}O_c$-based SST reconstructions due to inaccurate $\delta^{18}O_{sw}$ assumptions[8,31]. However, these studies did not account for seasonal biases.

Seasonal variability in growth rates in all specimens (**Fig 2A**) illustrates how bulk sampling of bio-archives can lead to significant biases in MAT reconstructions compared to our more accurate estimates of MAT as an average of Δ_{47}-based monthly SST. In this case, slower summer

and autumn growth (months 4-7 in **Fig. 2A**), especially in *A. incurva* and *B. suecicus*, would cause bulk analysis of shell material to underestimate MAT. Indeed, our Campanian mid-latitude SST ranges (~15-27°C, MAT of 20°C) are significantly higher than previous reconstructions of the same paleolatitude based on fish tooth $\delta^{18}O_c$ (15–20°C[11]), chalk $\delta^{18}O_c$ (12–15°C[12]), bulk mollusk Δ_{47} (5–12°C[32]), TEX_{86} (15–20°C[8]) and sub-annual mollusk $\delta^{18}O_c$ (15–22°C[10,26]; **Fig. 3A**). All these reconstructions are potentially affected by either seasonal or $\delta^{18}O_{sw}$ bias, or both. Our more accurate reconstructions of $\delta^{18}O_{sw}$ and SST on a seasonal scale aid in evaluating these biases and correct for them by combining long-term MAT reconstructions with snapshots of climate on the seasonal scale.

Given the increase in frequency and duration of growth stops in modern mollusks with increasing latitude[33], seasonal biases are likely more common in higher latitude environments. The accuracy of our new method for SST reconstruction and the remarkable agreement between Δ_{47}-based SST ranges and our climate model strongly suggest that the average seasonal range reconstructed from our three specimens (15-27°C range, MAT of 20°C) represents the most accurate SST seasonality reconstructions for the Campanian Boreal Chalk Sea to date. Since shallow marine bio-archives can record local climate conditions at higher spatial and temporal resolution than conventional (open ocean) archives, our monthly resolved Δ_{47} records showcase a tool for eliminating widespread biases related to seasonal variability and $\delta^{18}O_{sw}$ assumptions on SST reconstructions across time and space.

Robust agreement between our reconstructions and the 4× preindustrial pCO_2 model simulation down to the monthly scale provides strong evidence for considerably warmer (~8°C) higher latitudes during the Late Cretaceous greenhouse compared to the present day. Significant disagreement of summer, winter and annual SST reconstructions from every specimen in this study

with the 2× preindustrial pCO_2 simulation strongly favor warmer (4× preindustrial pCO_2) climate conditions (see **Supplementary Data 4**). Bio-archives from mid to high latitudes are likely much more sensitive to $\delta^{18}O_{sw}$ and seasonality bias than low-latitude records, contributing to the flawed paradigm of shallow latitudinal temperature gradients during greenhouse climates. Instead, our results concur with the recent trend of converging data and model reconstructions yielding modern-scale Late Cretaceous latitudinal temperature gradients[13], thereby challenging the hypothesis of "equable climate" during greenhouse periods[9]. Moreover, our unique absolute monthly SST reconstructions and model simulations corroborate growing evidence against the hypothesis of reduced temperature seasonality in greenhouse climates[30]. Future work should aim to further test these hypotheses by applying the clumped isotope seasonality method on bio-archives from a range of latitudes in greenhouse climate periods. Results from *B. suecicus* represent the first Δ_{47}-based SST reconstructions from rudist bivalves, introducing an abundant archive for accurate Mesozoic SST seasonality reconstructions with which these new insights can be evaluated.

Conclusions

Our new absolute temperature seasonality reconstructions merit critical evaluation of classical paleoclimate records that risk bias, such as those based on $\delta^{18}O_c$ (assuming constant $\delta^{18}O_{sw}$[7,10]), bulk analyses of fossil material with growth seasonality (e.g. mollusks and brachiopods[31]) or a fixed growth season (e.g. planktic foraminifera[36]) and organic proxies that may be seasonally biased (e.g. TEX_{86} and $U^{k'}_{37}$ [5,37]). In addition, our monthly $\delta^{18}O_{sw}$ reconstructions for the first time allow evaluation of local seasonality in the hydrological cycle from accretionary bio-archives, revealing dry summers and wet winters in the Campanian Kristianstad Basin. This unique advantage of Δ_{47}-based seasonality reconstructions enables the reconstruction of previously

unknown high-resolution variability in salinity, local rainfall and evaporation in past climates. Combined with longer-term, global-scale paleoclimate records and models, our new method for absolute monthly SST and $\delta^{18}O_{sw}$ reconstructions has the potential to resolve critical disagreements between SST proxies, reduce biases of deep-time paleoclimate reconstructions, shed light on new aspects of past climate seasonality and reconcile proxy reconstructions and model simulations of greenhouse climate.

MAIN REFERENCES

1. Marshall, D. J. & Burgess, S. C. Deconstructing environmental predictability: seasonality, environmental colour and the biogeography of marine life histories. *Ecology Letters* **18**, 174–181 (2015).
2. Matthews, T., Mullan, D., Wilby, R. L., Broderick, C. & Murphy, C. Past and future climate change in the context of memorable seasonal extremes. *Climate Risk Management* **11**, 37–52 (2016).
3. Carré, M. & Cheddadi, R. Seasonality in long-term climate change. *Quaternaire. Revue de l'Association française pour l'étude du Quaternaire* 173–177 (2017) doi:10.4000/quaternaire.8018.
4. Zeebe, R. E., Zachos, J. C. & Dickens, G. R. Carbon dioxide forcing alone insufficient to explain Palaeocene–Eocene Thermal Maximum warming. *Nature Geoscience* **2**, 576 (2009).
5. Cramwinckel, M. J. *et al.* Synchronous tropical and polar temperature evolution in the Eocene. *Nature* **559**, 382 (2018).

6. IPCC. *IPCC, 2013: Climate Change 2013: The Physical Science Basis. Contribution of Working Group I to the Fifth Assessment Report of the Intergovernmental Panel on Climate Change, 1535 pp*. (Cambridge Univ. Press, Cambridge, UK, and New York, 2013).
7. Jenkyns, H. C., Forster, A., Schouten, S. & Damsté, J. S. S. High temperatures in the late Cretaceous Arctic Ocean. *Nature* **432**, 888 (2004).
8. O'Brien, C. L. *et al.* Cretaceous sea-surface temperature evolution: Constraints from TEX 86 and planktonic foraminiferal oxygen isotopes. *Earth-Science Reviews* **172**, 224–247 (2017).
9. Huber, B. T., Hodell, D. A. & Hamilton, C. P. Middle–Late Cretaceous climate of the southern high latitudes: stable isotopic evidence for minimal equator-to-pole thermal gradients. *Geological Society of America Bulletin* **107**, 1164–1191 (1995).
10. Steuber, T., Rauch, M., Masse, J.-P., Graaf, J. & Malkoč, M. Low-latitude seasonality of Cretaceous temperatures in warm and cold episodes. *Nature* **437**, 1341–1344 (2005).
11. Pucéat, E. *et al.* Fish tooth δ18O revising Late Cretaceous meridional upper ocean water temperature gradients. *Geol* **35**, 107 (2007).
12. Thibault, N., Harlou, R., Schovsbo, N. H., Stemmerik, L. & Surlyk, F. Late Cretaceous (late Campanian–Maastrichtian) sea-surface temperature record of the Boreal Chalk Sea. *Climate of the Past* **12**, 429–438 (2016).
13. Upchurch Jr, G. R., Kiehl, J., Shields, C., Scherer, J. & Scotese, C. Latitudinal temperature gradients and high-latitude temperatures during the latest Cretaceous: Congruence of geologic data and climate models. *Geology* **43**, 683–686 (2015).
14. Farnsworth, A. *et al.* Climate Sensitivity on Geological Timescales Controlled by Nonlinear Feedbacks and Ocean Circulation. *Geophys. Res. Lett.* **46**, 9880–9889 (2019).

15. Joussaume, S. & Braconnot, P. Sensitivity of paleoclimate simulation results to season definitions. *Journal of Geophysical Research: Atmospheres* **102**, 1943–1956 (1997).

16. Mosbrugger, V. Nearest-living-relative method. *Encyclopedia of paleoclimatology and ancient environments* 607–609 (2009).

17. Kim, S.-T. & O'Neil, J. R. Equilibrium and nonequilibrium oxygen isotope effects in synthetic carbonates. *Geochimica et Cosmochimica Acta* **61**, 3461–3475 (1997).

18. Jaffrés, J. B. D., Shields, G. A. & Wallmann, K. The oxygen isotope evolution of seawater: A critical review of a long-standing controversy and an improved geological water cycle model for the past 3.4 billion years. *Earth-Science Reviews* **83**, 83–122 (2007).

19. Veizer, J. & Prokoph, A. Temperatures and oxygen isotopic composition of Phanerozoic oceans. *Earth-Science Reviews* **146**, 92–104 (2015).

20. de Winter, N., Agterhuis, T. & Ziegler, M. Optimizing sampling strategies in high-resolution paleoclimate records. Climate of the Past Discussions 1–52 (2020) doi:https://doi.org/10.5194/cp-2020-118.

21. Eiler, J. M. "Clumped-isotope" geochemistry—The study of naturally-occurring, multiply-substituted isotopologues. *Earth and Planetary Science Letters* **262**, 309–327 (2007).

22. Petersen, S. V. *et al.* Effects of Improved 17O Correction on Interlaboratory Agreement in Clumped Isotope Calibrations, Estimates of Mineral-Specific Offsets, and Temperature Dependence of Acid Digestion Fractionation. *Geochemistry, Geophysics, Geosystems* **20**, 3495–3519 (2019).

23. Bernasconi, S. M. et al. Reducing uncertainties in carbonate clumped isotope analysis through consistent carbonate-based standardization. Geochemistry, Geophysics, Geosystems 19, 2895–2914 (2018).

24. Jautzy, J. J., Savard, M. M., Dhillon, R. S., Bernasconi, S. M. & Smirnoff, A. Clumped isotope temperature calibration for calcite: Bridging theory and experimentation. Geochemical Perspectives Letters 14, 36–41 (2020).

25. Fernandez, A. *et al.* A reassessment of the precision of carbonate clumped isotope measurements: implications for calibrations and paleoclimate reconstructions. *Geochemistry, Geophysics, Geosystems* **18**, 4375–4386 (2017).

26. de Winter, N. J. *et al.* Shell chemistry of the boreal Campanian bivalve *Rastellum diluvianum* (Linnaeus, 1767) reveals temperature seasonality, growth rates and life cycle of an extinct Cretaceous oyster. *Biogeosciences* **17**, 2897–2922 (2020).

27. Surlyk, F. & Sørensen, A. M. An early Campanian rocky shore at Ivö Klack, southern Sweden. *Cretaceous Research* **31**, 567–576 (2010).

28. NOAA Global Surface Temperature (NOAAGlobalTemp) data provided by the NOAA/OAR/ESRL PSL, Boulder, Colorado, USA, https://psl.noaa.gov/, last accessed: 28/05/2020.

29. Huyghe, D. et al. New insights into oyster high-resolution hinge growth patterns. Mar Biol 166, 48 (2019).

30. Shackleton, N. J. Paleogene stable isotope events. *Palaeogeography, Palaeoclimatology, Palaeoecology* **57**, 91–102 (1986).

31. Tagliavento, M., John, C. M. & Stemmerik, L. Tropical temperature in the Maastrichtian Danish Basin: Data from coccolith Δ47 and δ18O. *Geology* **47**, 1074–1078 (2019).

32. Petersen, S. V. *et al.* Temperature and salinity of the Late Cretaceous western interior seaway. *Geology* **44**, 903–906 (2016).

33. Lartaud, F. *et al.* A latitudinal gradient of seasonal temperature variation recorded in oyster shells from the coastal waters of France and The Netherlands. *Facies* **56**, 13 (2009).

34. Burgener, L., Hyland, E., Huntington, K. W., Kelson, J. R. & Sewall, J. O. Revisiting the equable climate problem during the Late Cretaceous greenhouse using paleosol carbonate clumped isotope temperatures from the Campanian of the Western Interior Basin, USA. *Palaeogeography, Palaeoclimatology, Palaeoecology* **516**, 244–267 (2019).

35. Henkes, G. A. *et al.* Temperature evolution and the oxygen isotope composition of Phanerozoic oceans from carbonate clumped isotope thermometry. *Earth and Planetary Science Letters* **490**, 40–50 (2018).

36. Pearson, P. N. *et al.* Warm tropical sea surface temperatures in the Late Cretaceous and Eocene epochs. *Nature* **413**, 481–487 (2001).

37. Jia, G., Wang, X., Guo, W. & Dong, L. Seasonal distribution of archaeal lipids in surface water and its constraint on their sources and the TEX86 temperature proxy in sediments of the South China Sea. *Journal of Geophysical Research: Biogeosciences* **122**, 592–606 (2017).

38. Sørensen, A. M., Surlyk, F. & Jagt, J. W. M. Adaptive morphologies and guild structure in a high-diversity bivalve fauna from an early Campanian rocky shore, Ivö Klack (Sweden). *Cretaceous Research* **33**, 21–41 (2012).

Table 1: Overview of analytical results ($\delta^{18}O_c$ and Δ_{47}) and reconstructions

Species (locality)	age [yr]	Measurement results								Monthly reconstructions					
		$\delta^{18}O_c$ [‰VPDB]				Δ_{47} [‰]				$\delta^{18}O_{sw}$ [‰VSMOW]			SST [°C]		
		N [b]	*min.*	*mean*	*max*	*N*	*min.*	*mean*	*max*	*CM* [c]	*MA* [d]	*WM* [e]	*CM*	*MA*	*WM*
R. diluvianum **(Ivö Klack)**	6.2	198	**-2.08** *±0.08*	**-1.16** *±0.08*	**0.18** *±0.08*	121	**0.605** *±0.077*	**0.678** *±0.077*	**0.795** *±0.077*	**0.00** *±0.27*	**0.56** *±0.11*	**1.08** *±0.36*	**19.6** *±1.8*	**24.6** *±0.7*	**29.2** *±2.3*
A. incurva **(Åsen)**	3.3	150	**-2.26** *±0.08*	**-0.71** *±0.08*	**0.15** *±0.08*	115	**0.601** *±0.077*	**0.706** *±0.077*	**0.831** *±0.077*	**-0.89** *±0.18*	**-0.46** *±0.09*	**-0.36** *±0.87*	**12.7** *±2.3*	**16.4** *±0.7*	**25.7** *±4.2*
B. suecicus **(Maltesholm)**	3	178	**-2.93** *±0.08*	**-1.99** *±0.08*	**-0.98** *±0.08*	102	**0.565** *±0.077*	**0.688** *±0.077*	**0.779** *±0.077*	**-1.81** *±0.78*	**-1.18** *±0.17*	**-0.55** *±0.45*	**13.7** *±3.9*	**19.3** *±0.9*	**24.8** *±2.6*

N = Number of measurements and the age is estimated from the age modelling results (**Supplementary Data 1**), CM = Coldest Month, MA = Mean Annual, WM = Warmest Month. All uncertainties are given as 95% confidence levels.

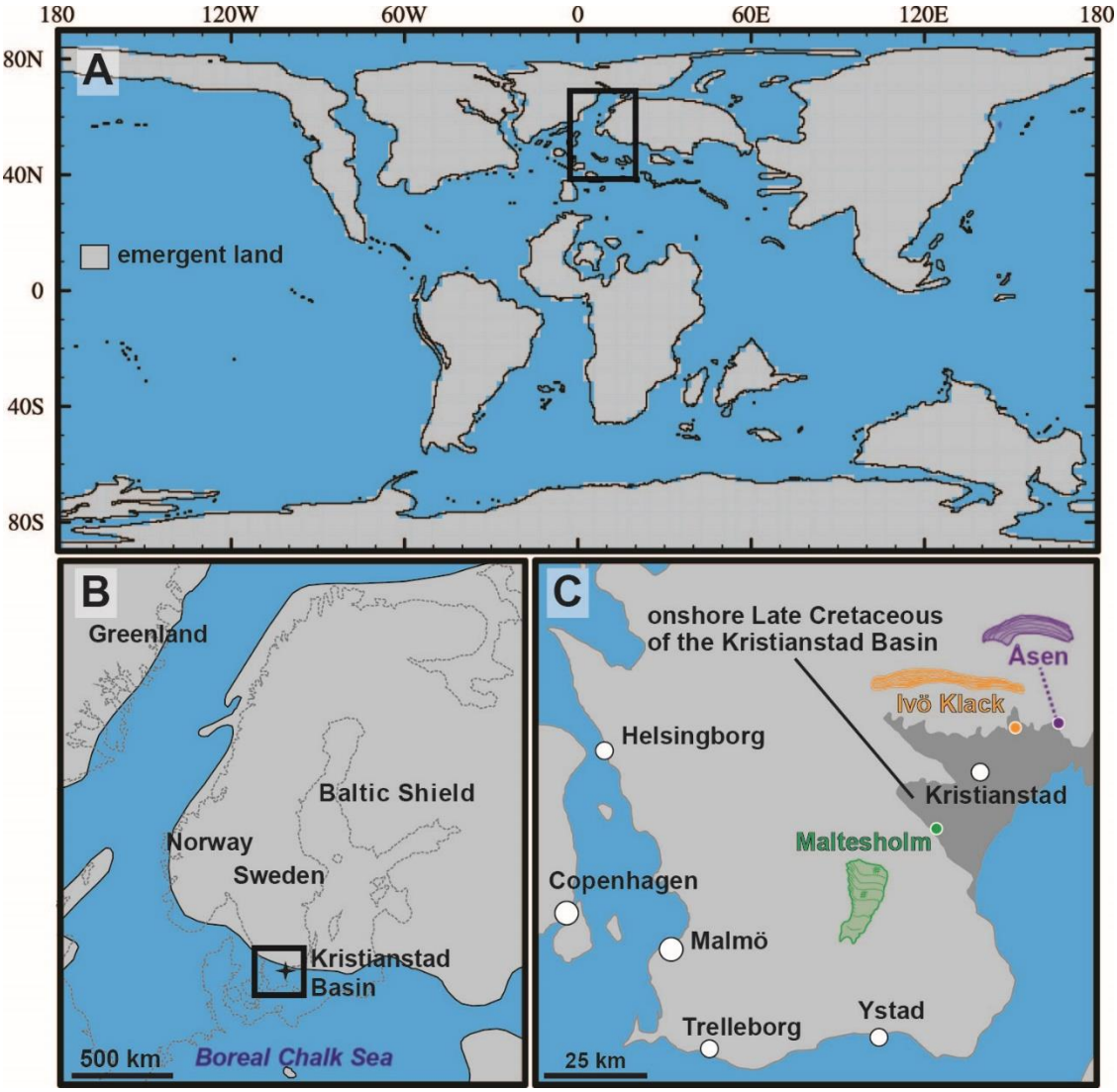

Fig. 1: **Campanian (78 Ma) paleogeography and geological setting A**) Global paleogeography used in climate model[14] **B**) Northern Europe, black star indicates the Kristianstad Basin **C**) Southern Sweden with Kristianstad Basin (in dark grey, submerged in the Campanian). Colored dots indicate the three sampled localities on the paleoshoreline with schematic representations of the species. In all maps, blue color indicates sea surface and light grey indicates emergent land. Maps **B**) and **C**) are adapted from[38].

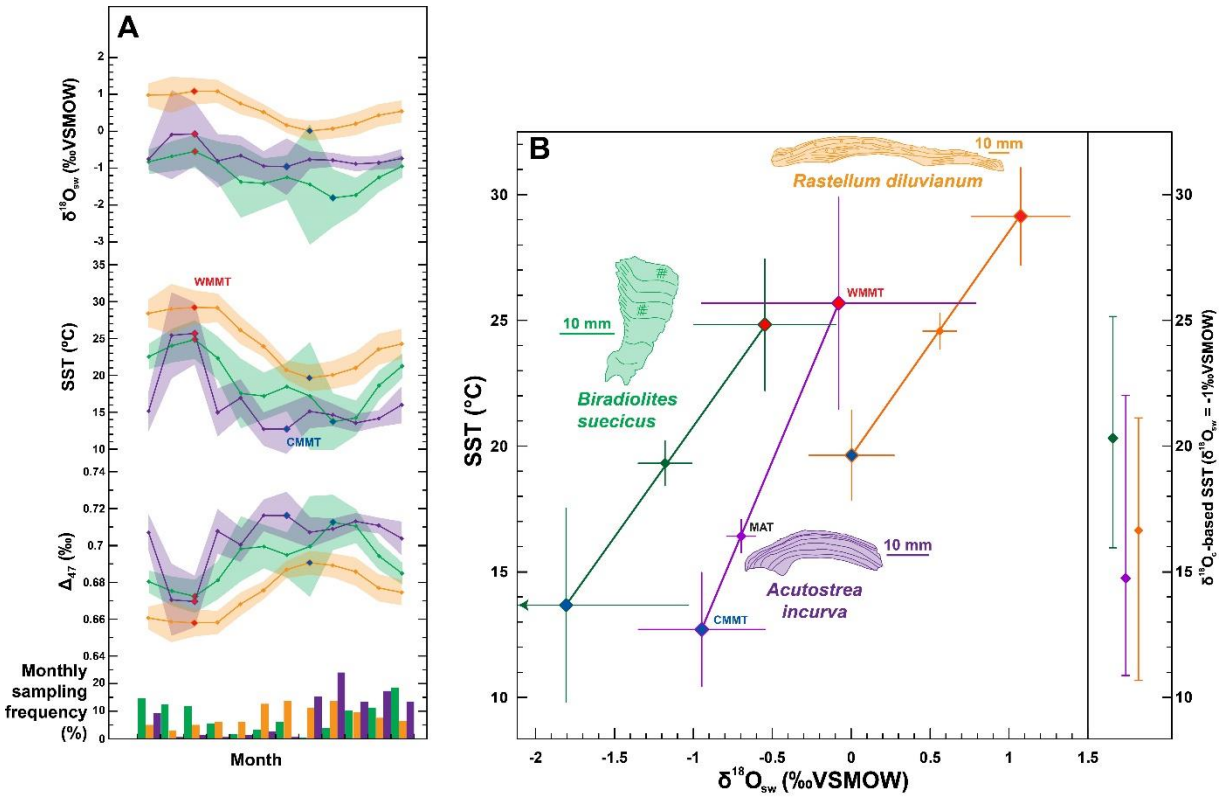

Fig. 2: **Paleoseasonality reconstructions A**) From bottom to top: relative monthly sampling frequencies reflecting growth rate variability (bar chart), monthly average Δ_{47}, SST and $\delta^{18}O_{sw}$ reconstructions from *R. diluvianum* (orange), *A. incurva* (purple) and *B. suecicus* (green). Shaded envelopes indicate 95% confidence levels. Red and blue dots respectively indicate warmest and coldest months. **B**) SST and $\delta^{18}O_{sw}$ reconstructions of warmest month (red symbols), coldest month (blue symbols) and annual average (symbols in color of specimen). Thin crosses indicate 95% confidence level uncertainties. Vertical bars on the right indicate summer, winter and MAT estimates from $\delta^{18}O_c$ (assuming constant $\delta^{18}O_{sw}$ of -1‰VSMOW). Scaled cross-sections through specimens are drawn with horizontal 10 mm scale bars.

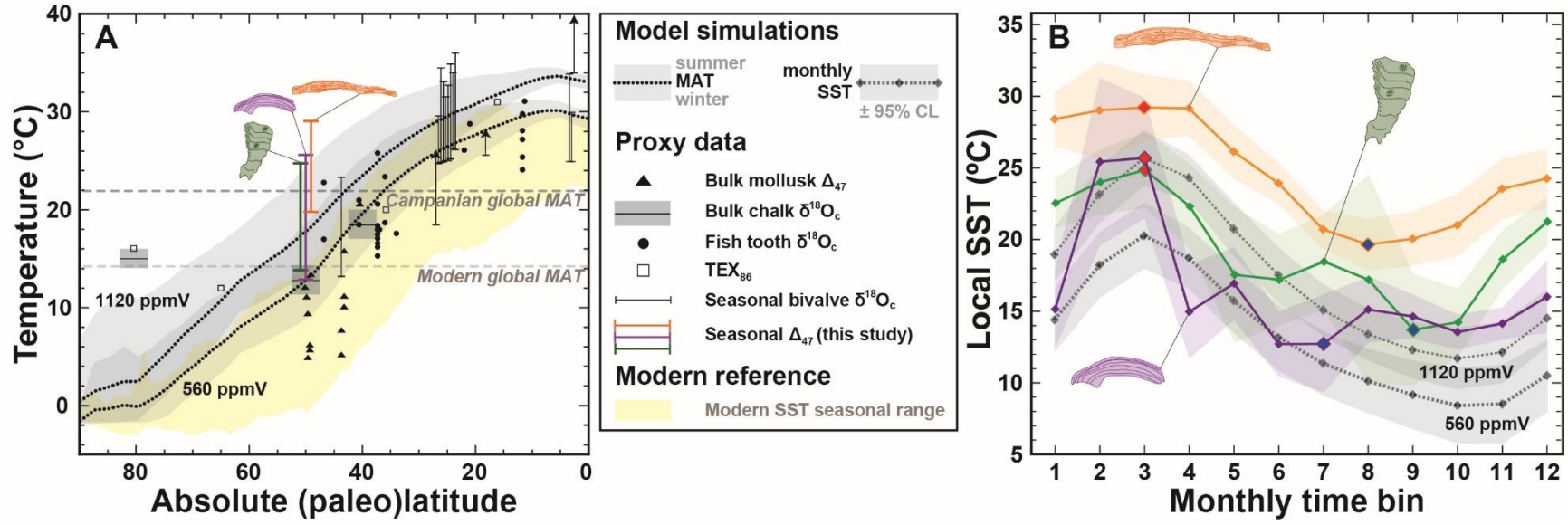

Fig. 3: **Comparison between model and reconstructions**. **A**) Campanian latitudinal SST gradient with vertical orange, purple and green bars showing seasonality reconstructions and dashed black lines indicating modeled mean annual temperatures (560 ppmV = 2× preindustrial and 1120 ppmV = 4× preindstrial pCO_2) with grey envelopes representing seasonality. Black symbols and bars show previous SST reconstructions[7,8,10,11,12,32,39,40]. The shaded yellow envelope indicates modern seasonal SST range[28]. Horizontal dashed lines mark modern and Campanian global MAT. **B**) Monthly SST reconstructions (in orange, purple and green) and local model outputs (in grey) in the Boreal Chalk Sea. Diamonds indicate monthly SST means, with red and blue diamonds showing monthly summer and winter extremes, respectively. Shaded envelopes show 95% confidence levels and color coding follows **Fig. 2**.

METHODS

Geological setting

The bivalve specimens used in this study were obtained from the Ivö Klack (*R. diluvianum*), Åsen (*A. incurva*) and Maltesholm (*B. suecicus*) localities in the Kristianstad Basin in southern Sweden (56°2' N, 14° 9' E; 46±3°N paleolatitude[27,41]; see **Fig. 1** and **Supplementary Data 7**). The three distinct localities contain a rich (> 200 species), well preserved Campanian rocky shore fauna[27,38] and were all deposited at the peak of transgression of the latest early Campanian, as supported by the restriction of these deposits to the *Belemnellocamax mammillatus* belemnite biozone and Sr-isotope chemostratigraphy[26,38,42]. The tectonic quiescence of the region since the Late Cretaceous limited burial and promoted excellent shell preservation[27]. Burial of loosely compacted sediments of the studied localities was limited to a maximum of 40 meters[27]. We can therefore conclude that burial temperatures never exceeded 80°C and that solid-state reordering did not affect clumped isotope results from these specimens[43,44] (see **Supplementary Methods**). The Kristianstad Basin represents the highest latitude location for the occurrence of rudist bivalves known to date[38].

Materials

Fossil *R. diluvianum* oysters were found *in situ* clinging to the sides of large boulders at a paleodepth of <5 m[27], while the *B. suecis* rudist and *A. incurva* oysters were found in life position in a deeper setting (5–15m) among skeletal fragments on the paleo-seafloor[45] (see **Supplementary Methods**). The preservation of multiple specimens from this site (including the ones used here) was demonstrated through electron and visible light microscopy, trace element (e.g. Sr/Ca and

Mn/Ca) analyses and ultrastructure preservation, results of which are reported in detail in [26] and [45] and summarized in **Supplementary Methods**.

Sampling

Powdered samples (~300 µg) were drilled in growth direction from polished cross sections through the shell's axis of maximum growth using a Dremel® 3000 rotary drill (Robert Bosch Ltd., Uxbridge, UK) operated at slow rotation equipped with a 300 µm wide tungsten carbide drill bit. High (~100 µm) uniform sampling resolution was achieved by careful abrasive drilling using the side of the drill parallel to the growth lines in the shell. In oyster shells, the well-preserved dense foliated calcite was targeted, while in the rudist the dense outer calcite was sampled, avoiding the honeycomb structure in the inner part of the outer shell layer which is more susceptible to diagenetic alteration[46]. A total of 145 samples was obtained, from which 338 aliquots of ~100 µg were analyzed (see **Table 1**).

Clumped isotope analyses

Clumped isotope (Δ_{47}) analyses were carried out on Thermo Fisher Scientific MAT253 and 253 Plus mass spectrometers coupled to a Kiel IV carbonate preparation devices. Calcite samples (individual replicates of ~90 µg for MAT253 Plus and ~150 µg for MAT253) were reacted at 70 °C with nominally anhydrous (103%) phosphoric acid. The resulting CO_2 gas was cleaned from water and organic compounds with two cryogenic LN2 traps and a PoraPak Q trap kept at −40 °C. The purified sample gases were analyzed in micro-volume LIDI mode with 400 s integration time against a clean CO_2 working gas ($\delta^{13}C$ = -2.82‰; $\delta^{18}O$ = -4.67‰), corrected for the pressure baseline[41,42] and converted into the absolute reference frame by creating an empirical transfer function from the daily analyzed ETH calcite standards (ETH-1, -2, -3) and their accepted values[49].

All isotope data were calculated using the new IUPAC parameters following [49] and Δ_{47} values were projected to a 25 °C acid reaction temperature with a correction factor of 0.071 ‰[22]. Long-term Δ_{47} reproducibility standard deviation was 0.04‰ (0.039‰ for MAT253 Plus and 0.045‰ for MAT253) based on repeated measurements of ~100 µg aliquots of our check standard IAEA C2 (Δ_{47} of 0.719‰; measured over a 20-month period; see **Supplementary Data 8** for details). No statistical difference was found between results from both instruments (see **Supplementary Data 8**). For the $\delta^{18}O_c$ compositions we applied an acid correction factor of 1.00871[17] and reported versus VPDB with a typical reproducibility below 0.13‰ (95% confidence level). Results were combined with $\delta^{18}O_c$ data previously measured in the same shells[26,45] (**Supplementary Data 2**) to improve the confidence of seasonal age models and the temporal resolution of SST and $\delta^{18}O_{sw}$ reconstructions.

Absolute paleoseasonality reconstructions

We reconstructed absolute SST seasonality by aligning Δ_{47} data relative to the seasonal cycle observed in $\delta^{18}O_c$ using an age modelling routine[51] (**Supplementary Data 1 and 9**). Note that while chronologies were based on seasonal oscillations in $\delta^{18}O_c$ records, the resulting age model is not compromised by unconstrained seasonal variability in $\delta^{18}O_{sw}$ (see discussion in **[REF20]** and **Supplementary Methods**). Since only the shape of the seasonally oscillations in $\delta^{18}O_c$ is used for age modelling, age model results are independent on the absolute SST and $\delta^{18}O_{sw}$ seasonality and yield accurate results as long as the shape of the $\delta^{18}O_c$ curve exhibits annual cyclicity (see [50] and [20]; **Supplementary Methods**). We used a statistical approach to combine aliquots for Δ_{47}-based seasonality reconstructions. A step-by-step explanation of our Δ_{47}- $\delta^{18}O_c$ seasonality routine as well as a detailed evaluation of its precision and accuracy on a range of Δ_{47}- $\delta^{18}O_c$ datasets is

414 provided in [20] and in **Supplementary Methods**. The number of 100 µg Δ_{47} aliquots to combine
415 into monthly SST estimates is optimized by grouping aliquots from the same month in different
416 growth years. Analytical uncertainties are propagated through this optimization procedure using
417 Monte Carlo simulations (details in **Supplementary Methods** and **Supplementary Data 10**).
418 SST's are calculated from Δ_{47} values in monthly time bins ($1/12^{th}$ of the seasonal cycle) using the
419 temperature calibration by [51] recalculated in [23], and $\delta^{18}O_{sw}$ is reconstructed from Δ_{47}-SST and $\delta^{18}O_c$
420 following [17] (**Supplementary Methods** and **Supplementary Data 3**). The accuracy of this
421 statistical approach for combining Δ_{47} aliquots for seasonal SST and $\delta^{18}O_{sw}$ reconstructions is
422 tested on a diverse group of modern datasets and evaluated in [20]. It is demonstrated that this method
423 achieves the ideal compromise between eliminating bias and retaining high reproducibility while
424 keeping SST and $\delta^{18}O_{sw}$ reconstructions independent of the $\delta^{18}O_c$ values on which the age model
425 is based[20] (see also **Supplementary Methods**). The clumped isotope temperature calibration by [23]
426 is statistically indistinguishable from the temperature relationship based on theoretical principles
427 within the temperature range discussed in [24] and is the culmination of recent convergence of
428 measurement results between labs across the world and inter-lab standardization efforts[22,49].
429 Seasonality is defined as the difference between the average temperatures in the warmest and
430 coldest month, while mean annual temperature (MAT) is expressed as the average of all monthly
431 temperatures, following USGS definitions[52]. Statistical analyses of seasonality, differences
432 between specimens and differences between data and model are summarized in **Supplementary**
433 **Data 4**.
434
435 **Climate model**

We utilize a fully equilibrated (>11,000 model years) paleoclimate model (HadCM3L) Campanian (78 Ma) simulation. Model boundary conditions (topography, bathymetry, solar luminosity) for the Campanian are the same as in [14]. We evaluate model simulations with radiative forcing (pCO_2) set to 560 ppmV (2× preindustrial concentration) and 1120 ppmV (4× preindustrial concentration), within the range of pCO_2 reconstructions for the Campanian as compiled by [53], and a modern astronomical configuration with dynamic vegetation. Details on the HadCM3L model are provided in **Supplementary Methods** and in [14]. Local seasonal SSTs are calculated for the paleorotated Kristianstad Basin[41] (42.5-50°N, 7.5-15°E; **Supplementary Data 5**) from averages of the upper ocean grid boxes in the model simulation. The model has a spatial resolution of 3.75° × 2.5° and uses 20 layers in ocean depth, of which the upper ocean box averages the top 10 meters of the ocean. Hence the average SST of the Kristianstad Basin is biased against the shallowest coastal regions of the basin, such as the locality of *R. diluvianum*[54,55]. For comparison, modern SST data come from the National Oceanic and Atmospheric Administration[25] (**Supplementary Data 6** and **Supplementary Methods**).

Data availability

Extended methods, data and scripts belonging to this study are available in the open-access database Zenodo (https://doi.org/10.5281/zenodo.3865428).

METHODS REFERENCES

39. de Winter, N. J. *et al.* Tropical seasonality in the late Campanian (late Cretaceous): Comparison between multiproxy records from three bivalve taxa from Oman. *Palaeogeography, Palaeoclimatology, Palaeoecology* **485**, 740–760 (2017).

40. Walliser, E. O., Mertz-Kraus, R. & Schöne, B. R. The giant inoceramid Platyceramus platinus as a high-resolution paleoclimate archive for the Late Cretaceous of the Western Interior Seaway. *Cretaceous Research* **86**, 73–90 (2018).

41. van Hinsbergen, D. J. *et al.* A paleolatitude calculator for paleoclimate studies. *PloS one* **10**, e0126946 (2015).

42. Christensen, W. K. Paleobiogeography and migration in the Late Cretaceous belemnite family Belemnitellidae. *Acta palaeontologica polonica* **42**, 457–495 (1997).

43. Fernandez, A. et al. Reconstructing the magnitude of Early Toarcian (Jurassic) warming using the reordered clumped isotope compositions of belemnites. Geochimica et Cosmochimica Acta (2020) doi:10.1016/j.gca.2020.10.005.

44. Henkes, G. A. et al. Temperature limits for preservation of primary calcite clumped isotope paleotemperatures. Geochimica et Cosmochimica Acta 139, 362–382 (2014).

45. Sørensen, A. M., Ullmann, C. V., Thibault, N. & Korte, C. Geochemical signatures of the early Campanian belemnite Belemnellocamax mammillatus from the Kristianstad Basin in Scania, Sweden. *Palaeogeography, palaeoclimatology, palaeoecology* **433**, 191–200 (2015).

46. Pons, J. M. & Vicens, E. The structure of the outer shell layer in radiolitid rudists, a morphoconstructional approach. *Lethaia* **41**, 219–234 (2008).

47. Bernasconi, S. M. *et al.* Background effects on Faraday collectors in gas-source mass spectrometry and implications for clumped isotope measurements. *Rapid Communications in Mass Spectrometry* **27**, 603–612 (2013).

48. Meckler, A. N., Ziegler, M., Millán, M. I., Breitenbach, S. F. & Bernasconi, S. M. Long-term performance of the Kiel carbonate device with a new correction scheme for clumped isotope measurements. *Rapid Communications in Mass Spectrometry* **28**, 1705–1715 (2014).

49. Daëron, M., Blamart, D., Peral, M. & Affek, H. P. Absolute isotopic abundance ratios and the accuracy of Δ47 measurements. *Chemical Geology* **442**, 83–96 (2016).

50. Judd, E. J., Wilkinson, B. H. & Ivany, L. C. The life and time of clams: Derivation of intra-annual growth rates from high-resolution oxygen isotope profiles. *Palaeogeography, Palaeoclimatology, Palaeoecology* **490**, 70–83 (2018).

51. Kele, S. *et al.* Temperature dependence of oxygen-and clumped isotope fractionation in carbonates: a study of travertines and tufas in the 6–95 C temperature range. *Geochimica et Cosmochimica Acta* **168**, 172–192 (2015).

52. O'Donnell, M. S. & Ignizio, D. A. Bioclimatic predictors for supporting ecological applications in the conterminous United States. *US Geological Survey Data Series* **691**, (2012).

53. Foster, G. L., Royer, D. L. & Lunt, D. J. Future climate forcing potentially without precedent in the last 420 million years. *Nature Communications* **8**, 14845 (2017).

54. Johns, T. C. et al. The second Hadley Centre coupled ocean-atmosphere GCM: model description, spinup and validation. Climate Dynamics 13, 103–134 (1997).

55. Lunt, D. J. et al. Palaeogeographic controls on climate and proxy interpretation. Climate of the Past 12, (2016).

ACKNOWLEDGEMENTS

The authors thank Prof. Ethan Grossman and 2 anonymous reviewers for their comments that have helped improve the manuscript, as well as dr. Erin Scott for moderating the review process.

NJW is funded by the Flemish Research Council (FWO; junior postdoc grant; 12ZB220N) and the European Commission (MSCA Individual Fellowship; UNBIAS project 843011). NT acknowledges Carslbergfondet CF16-0457. PC would like to acknowledge funding from the VUB Strategic Research grant (internal). The authors would like to thank Bart Lippens for help with sample preparation, Arnold van Dijk for analytical support and Anne Sørensen for helping with sample collection.

AUTHOR CONTRIBUTIONS

The initial design of the study was conceived by NJW, NT, CVU and MZ. NJW, IAM, IJK and MZ together were responsible for clumped isotope data acquisition. NT and CVU provided samples used in this study. DJL and AF ran the climate model and provided in-depth input on model-data integration. NJW and PC were responsible for acquiring the funding needed for this study. NJW wrote the first draft of the manuscript and revision. All authors then contributed to the writing process.

COMPETING INTEREST DECLARATION

The authors have no competing interest to declare.

SUPPLEMENTARY INFORMATION

All supplementary material belonging to this manuscript is deposited in the open-source online database Zenodo (https://doi.org/10.5281/zenodo.3865428).

Figures

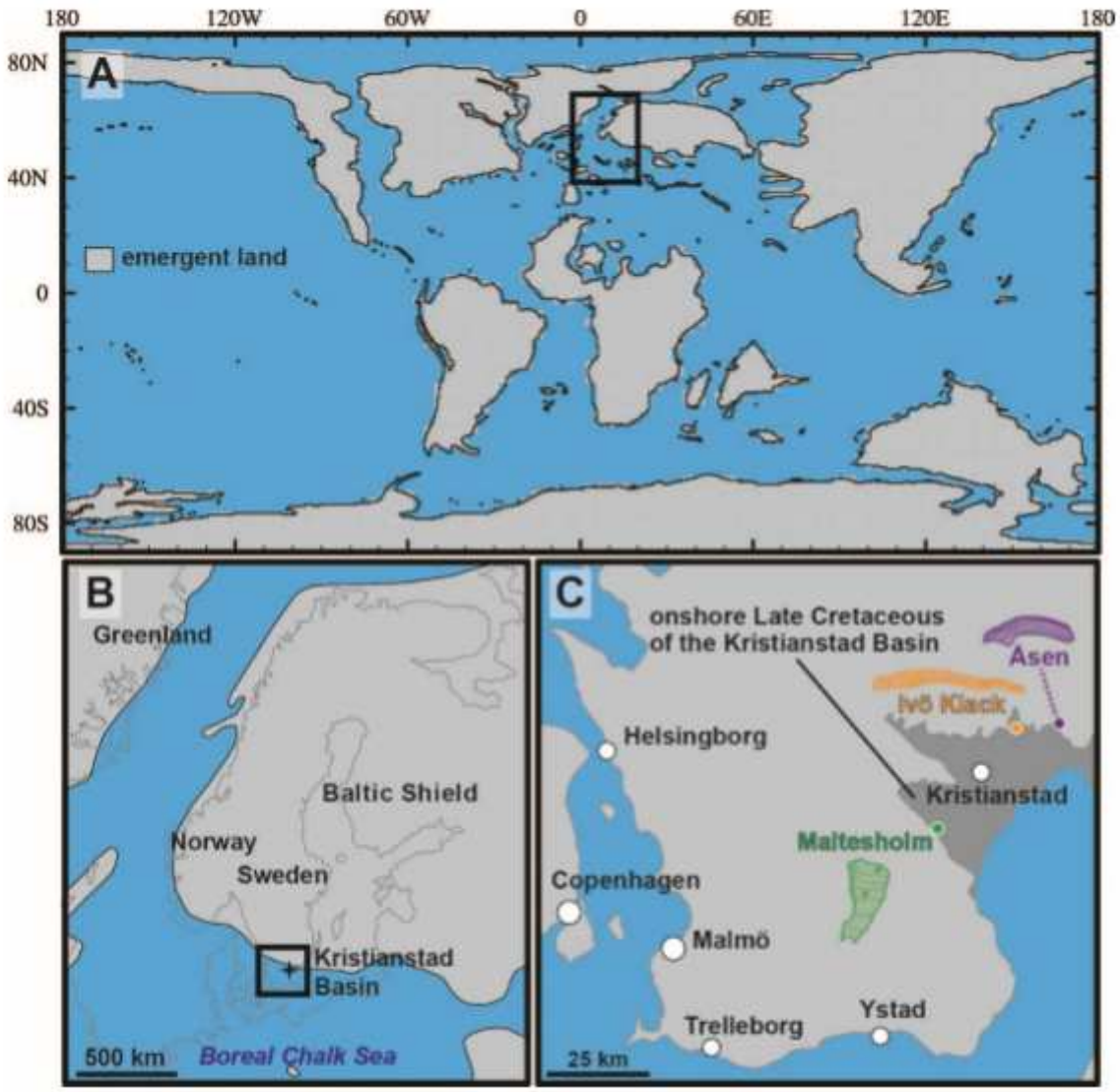

Figure 1

Campanian (78 Ma) paleogeography and geological setting A) Global paleogeography used in climate model14 B) Northern Europe, black star indicates the Kristianstad Basin C) Southern Sweden with Kristianstad Basin (in dark grey, submerged in the Campanian). Colored dots indicate the three sampled localities on the paleoshoreline with schematic representations of the species. In all maps, blue color indicates sea surface and light grey indicates emergent land. Maps B) and C) are adapted from38. Note: The designations employed and the presentation of the material on this map do not imply the expression of any opinion whatsoever on the part of Research Square concerning the legal status of any country, territory, city or area or of its authorities, or concerning the delimitation of its frontiers or boundaries. This map has been provided by the authors.

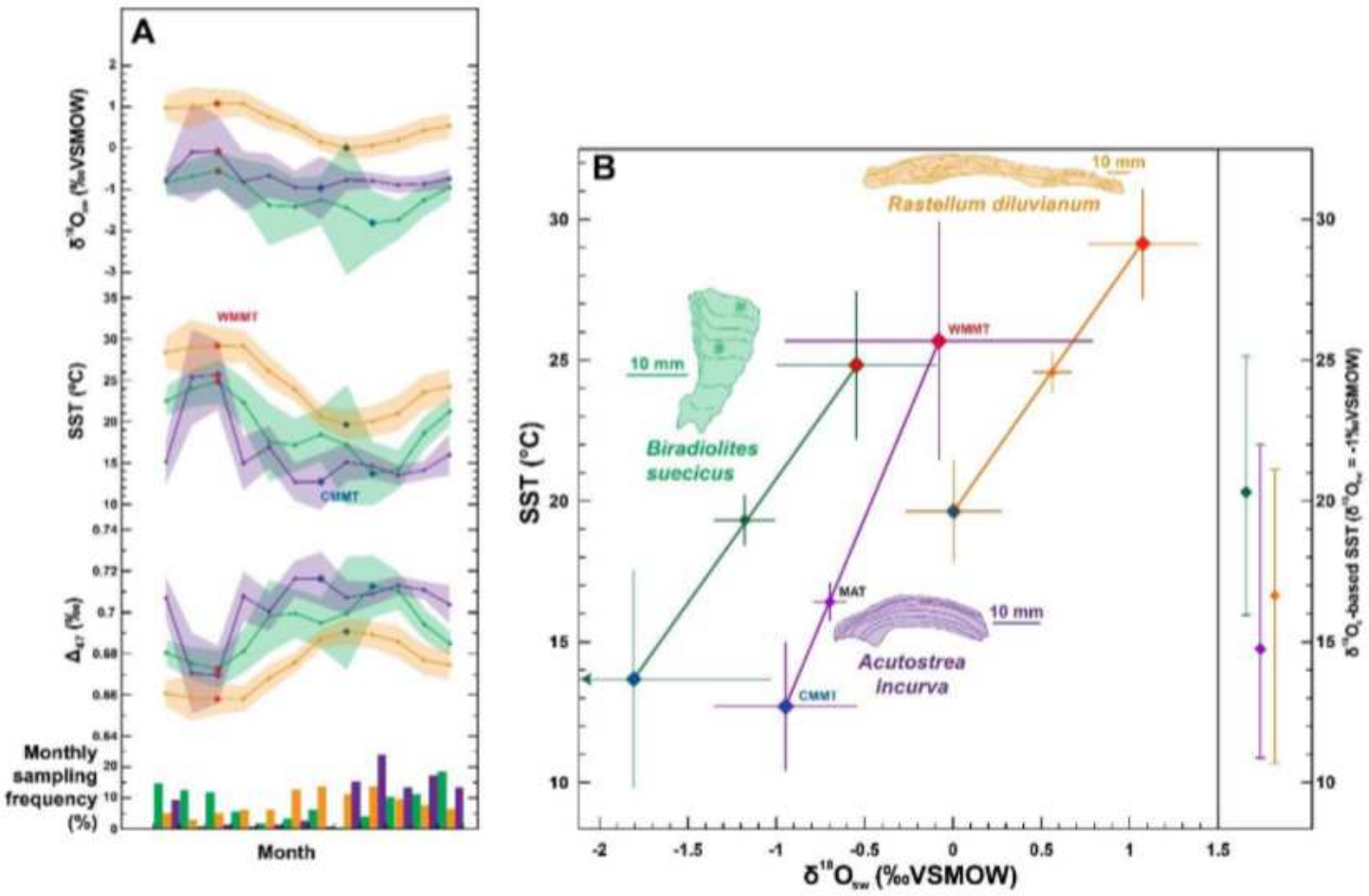

Figure 2

Paleoseasonality reconstructions A) From bottom to top: relative monthly sampling frequencies reflecting growth rate variability (bar chart), monthly average Δ47, SST and δ18Osw reconstructions from R. diluvianum (orange), A. incurva (purple) and B. suecicus (green). Shaded envelopes indicate 95% confidence levels. Red and blue dots respectively indicate warmest and coldest months. B) SST and δ18Osw reconstructions of warmest month (red symbols), coldest month (blue symbols) and annual average (symbols in color of specimen). Thin crosses indicate 95% confidence level uncertainties. Vertical bars on the right indicate summer, winter and MAT estimates from δ18Oc (assuming constant δ18Osw of -1‰VSMOW). Scaled cross-sections through specimens are drawn with horizontal 10 mm scale bars.

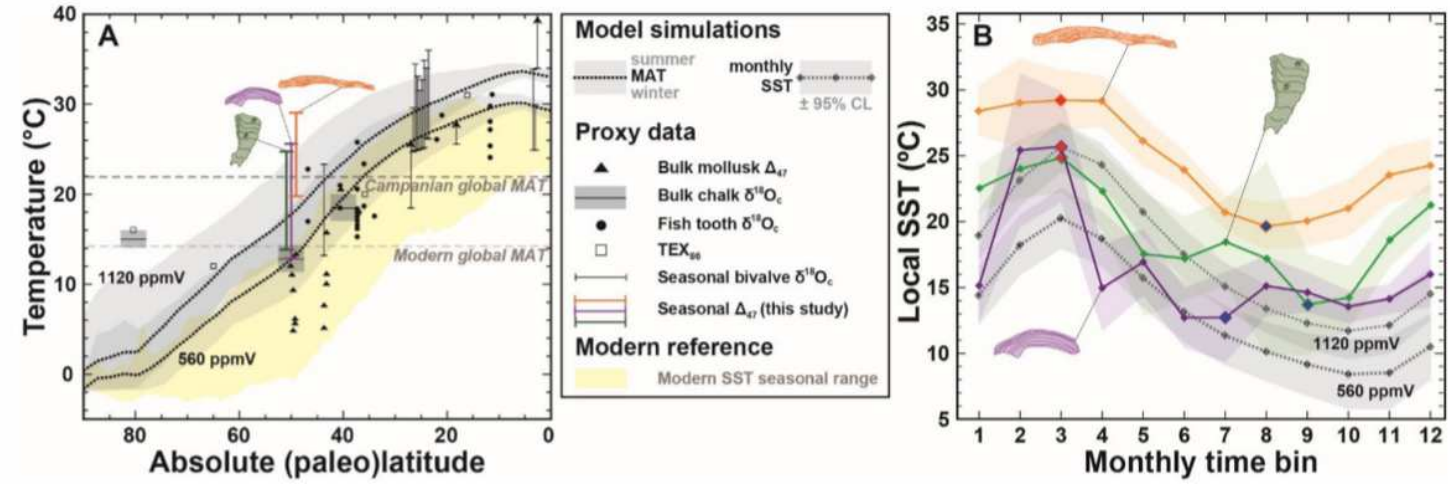

Figure 3

Comparison between model and reconstructions. A) Campanian latitudinal SST gradient with vertical orange, purple and green bars showing seasonality reconstructions and dashed black lines indicating modeled mean annual temperatures (560 ppmV = 2× preindustrial and 1120 ppmV = 4× preindstrial pCO2) with grey envelopes representing seasonality. Black symbols and bars show previous SST reconstructions7,8,10,11,12,32,39,40. The shaded yellow envelope indicates modern seasonal SST range28. Horizontal dashed lines mark modern and Campanian global MAT. B) Monthly SST reconstructions (in orange, purple and green) and local model outputs (in grey) in the Boreal Chalk Sea. Diamonds indicate monthly SST means, with red and blue diamonds showing monthly summer and winter extremes, respectively. Shaded envelopes show 95% confidence levels and color coding follows Fig. 2.

Supplementary Files

This is a list of supplementary files associated with this preprint. Click to download.

- SupplementaryTextNatCommEarthEnv.pdf